nature energy

SUPPLEMENTARY INFORMATION

https://doi.org/10.1038/s41560-019-0406-2

In the format provided by the authors and unedited.

Reduction of lead leakage from damaged lead halide perovskite solar modules using self-healing polymer-based encapsulation

Yan Jiang[1,2,3], Longbin Qiu[1,3], Emilio J. Juarez-Perez[1], Luis K. Ono[1], Zhanhao Hu[1], Zonghao Liu[1], Zhifang Wu[1], Lingqiang Meng[1], Qijing Wang[1] and Yabing Qi[1*]

[1]Energy Materials and Surface Sciences Unit, Okinawa Institute of Science and Technology Graduate University, Okinawa, Japan. [2]Present address: Laboratory for Thin Films and Photovoltaics, Swiss Federal Laboratories for Materials Science and Technology, Dübendorf, Switzerland. [3]These authors contributed equally: Yan Jiang, Longbin Qiu. *e-mail: Yabing.Qi@OIST.jp

SUPPLEMENTARY INFORMATION

Reduction of lead leakage from damaged lead halide perovskite solar modules using self-healing polymer-based encapsulation

Yan Jiang[†,§], Longbin Qiu[†], Emilio J. Juarez-Perez, Luis K. Ono, Zhanhao Hu, Zonghao Liu, Zhifang Wu, Lingqiang Meng, Qijing Wang, Yabing Qi*

Energy Materials and Surface Sciences Unit (EMSSU), Okinawa Institute of Science and Technology Graduate University (OIST), 1919-1 Tancha, Onna-son, Kunigami-gun, Okinawa, 904-0495, Japan

[§]Present address: Laboratory for Thin Films & Photovoltaics, Swiss Federal Laboratories for Materials Science and Technology (Empa), Überland Str. 129, 8600 Dübendorf, Switzerland

[†]These authors contributed equally to this work.

* E-mail: Yabing.Qi@OIST.jp (Y.B.Q.)

Supplementary Figures:

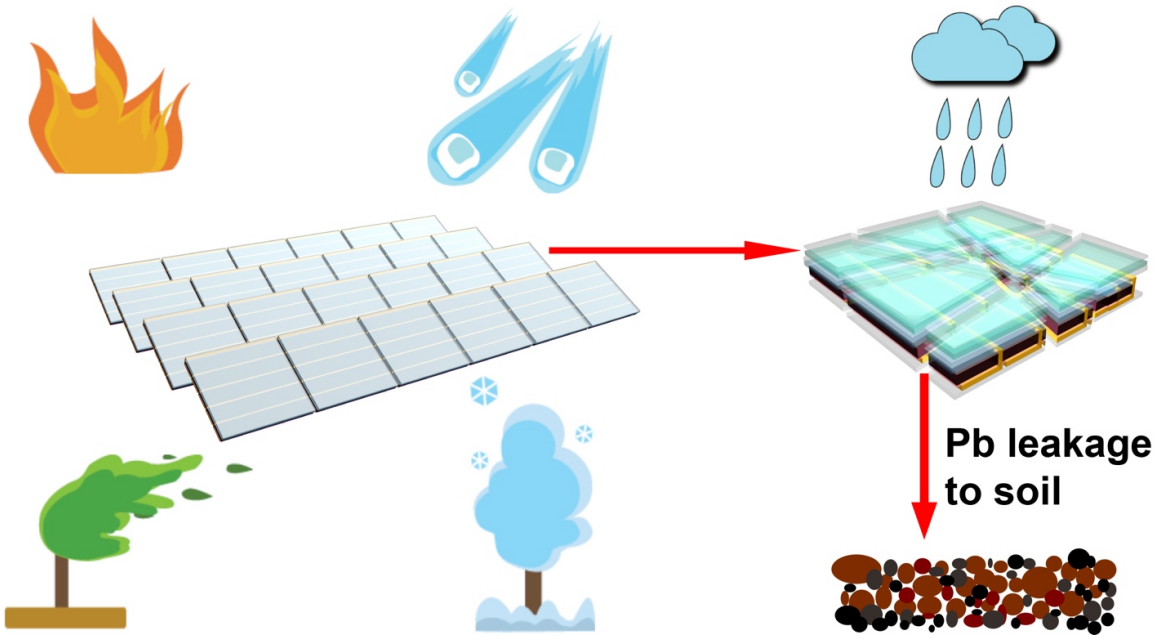

Supplementary Figure 1 | Schematic drawing showing the Pb leakage from perovskite solar modules. Perovskite solar modules for outdoor applications can get damaged or even broken due to natural causes e.g., hailstones, snow and wind loading, or fires during usage. The toxic Pb can leak from the damaged region during rainfall and contaminate the local environment.

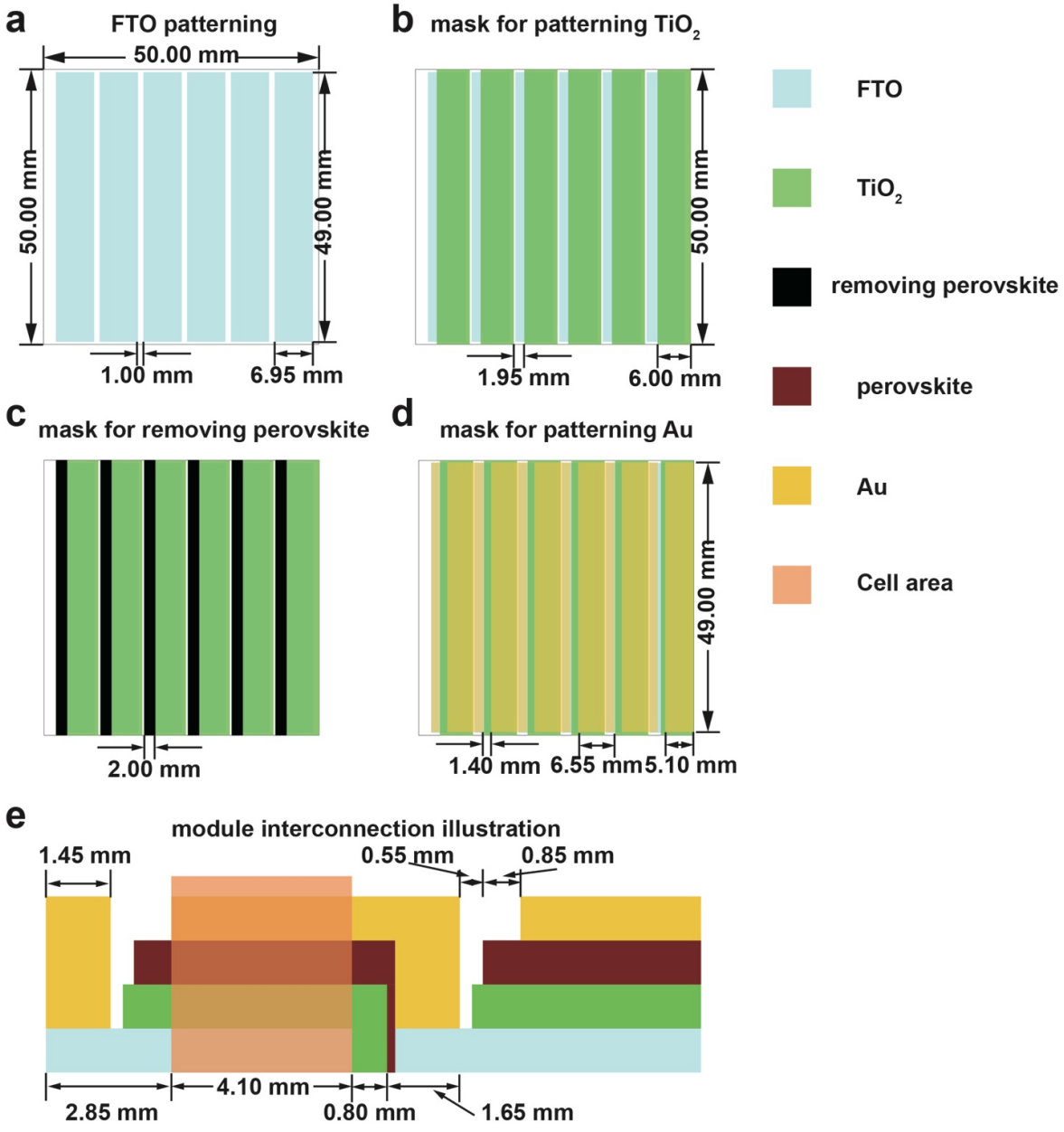

Supplementary Figure 2 | Schematic drawing showing the geometry of the perovskite solar module. (**a**) FTO patterning. Masks for (**b**) patterning TiO_2, (**c**) removing the perovskite, and (**d**) patterning Au. (**e**) Cross-section view illustration showing the solar module interconnections. The size of a single solar cell is 2.0 cm^2 and the size of the solar module is 12.0 cm^2.

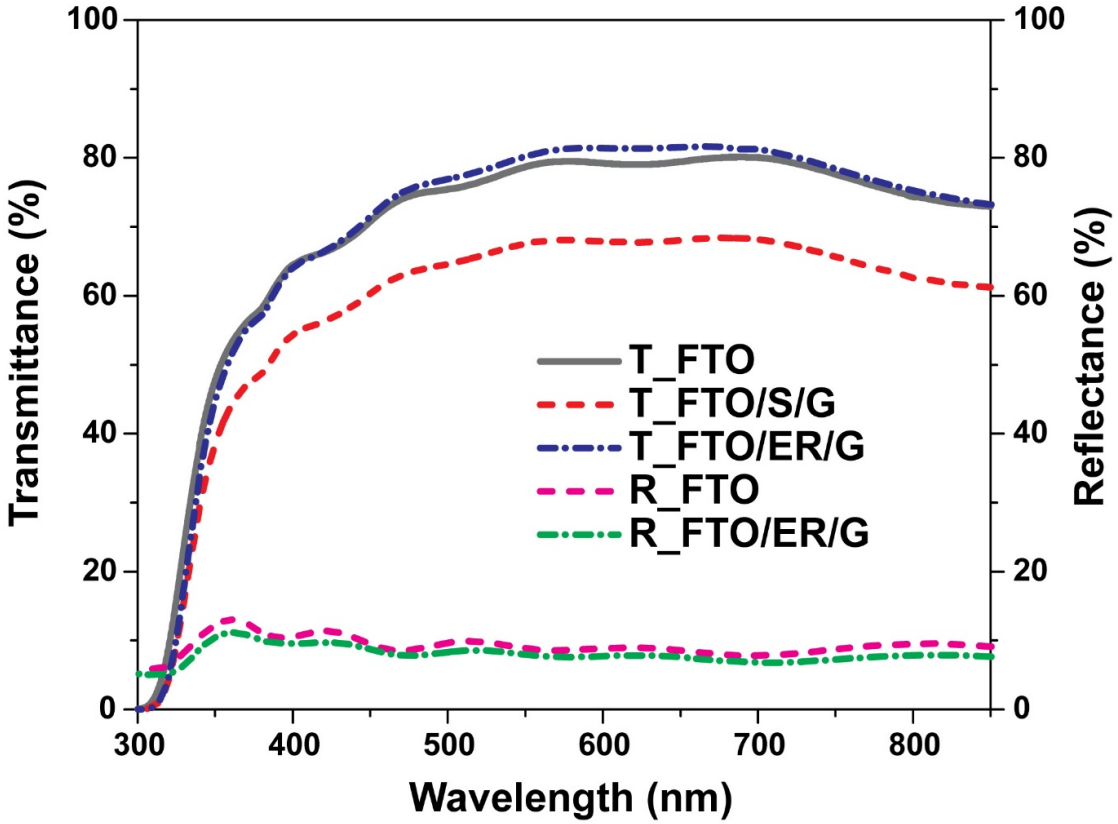

Supplementary Figure 3 | Transmittance and reflectance of the substrates. FTO glass, FTO glass with a surlyn film with a thickness of 80 μm and 1 mm-thick glass on top (FTO/S/G), FTO glass with an ER film with a thickness of 80 μm and 1 mm-thick glass on top (FTO/ER/G). Transmittance is significantly reduced after adding the surlyn film and the top glass cover on top of FTO. On the other hand, transmittance and reflectance after adding the ER film and a top glass cover are similar to the case of bare FTO.

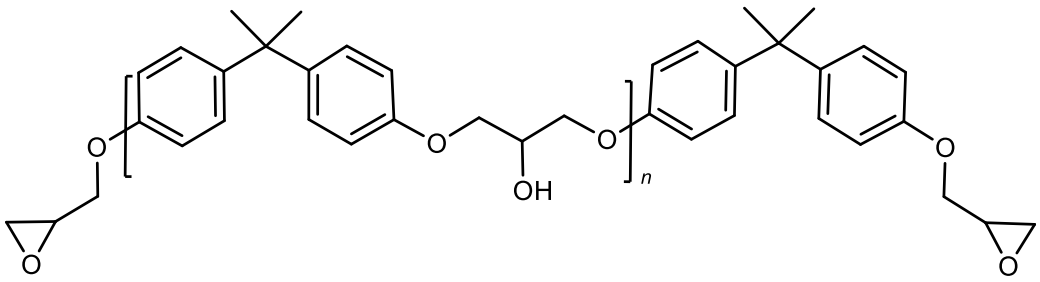

Diglycidyl ether of bisphenol A type epoxy resin E-51 (DGEBA)

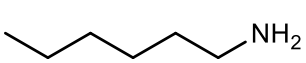

n-octylamine (OA)

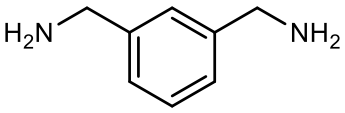

M-xylylenediamine (MXDA)

Polymerization

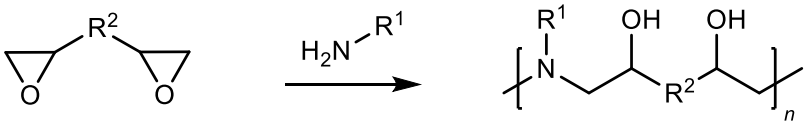

Supplementary Figure 4 | Polymerization of ER.

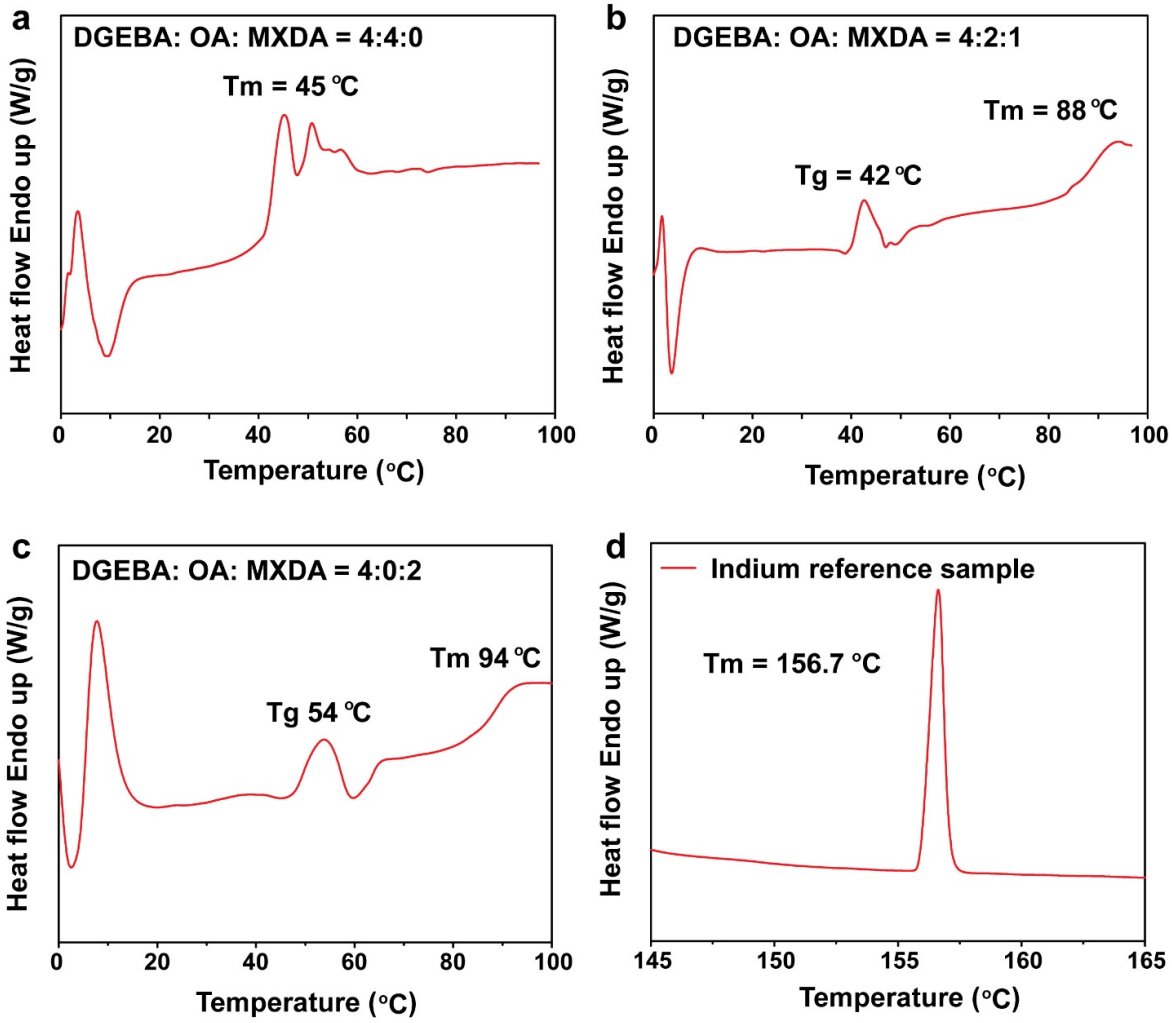

Supplementary Figure 5 | DSC curves of ER films. The different ratios of DGEBA: OA: MXDA in the ER films are (**a**) 4:4:0, (**b**) 4:2:1, (**c**) 4:0:2, respectively. (**d**) An indium reference sample showing a melting temperature (Tm) of 156.7 °C, which is consistent with the reference data sheet to confirm the normal working of equipment. Fluctuation lower than 20 °C is the background noise. The glass transition temperature (Tg) increases from less than 15 °C when the ratio of DGEBA: OA: MXDA is 4: 4: 0 (i.e., the linear ER), to 42 °C when the ratio of DGEBA: OA: MXDA is 4: 2: 1, and further to 54 °C when the ratio of DGEBA: OA: MXDA is 4: 0: 2. Tm also increases from 45 °C to 88 °C, and further to 94 °C, respectively. Increment of Tm is also demonstrated by increased mechanical strength, which is shown in the Supplementary Videos 1 and 2.

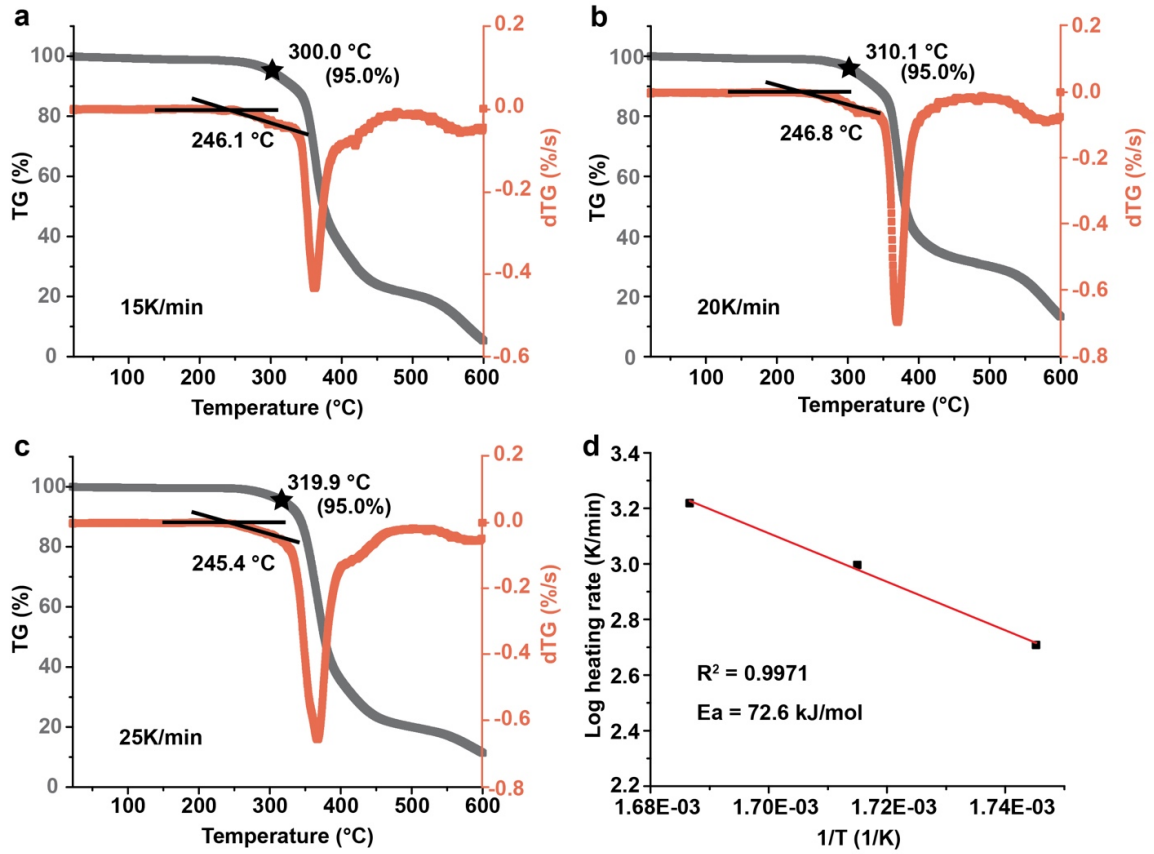

Supplementary Figure 6 | Thermal stability of the ER film. Thermal gravimetric analysis of the ER film with heating rates of (**a**) 15 K/min, (**b**) 20 K/min and (**c**) 25 K/min. (**d**) heating rate versus temperature figure. This approach assumes the Arrhenius behavior and first order reaction kinetics from 0 to 5 % of burn out of the ER film. The degradation temperature is 246.1 ºC, determined by the slope change of the differential thermogravimetry (dTG) traces at different scan rates. Activation energy (Ea) corresponding to thermal decomposition of the ER film is 72.6 kJ/mol, determined by fitting the decomposition temperatures at different heating rates.

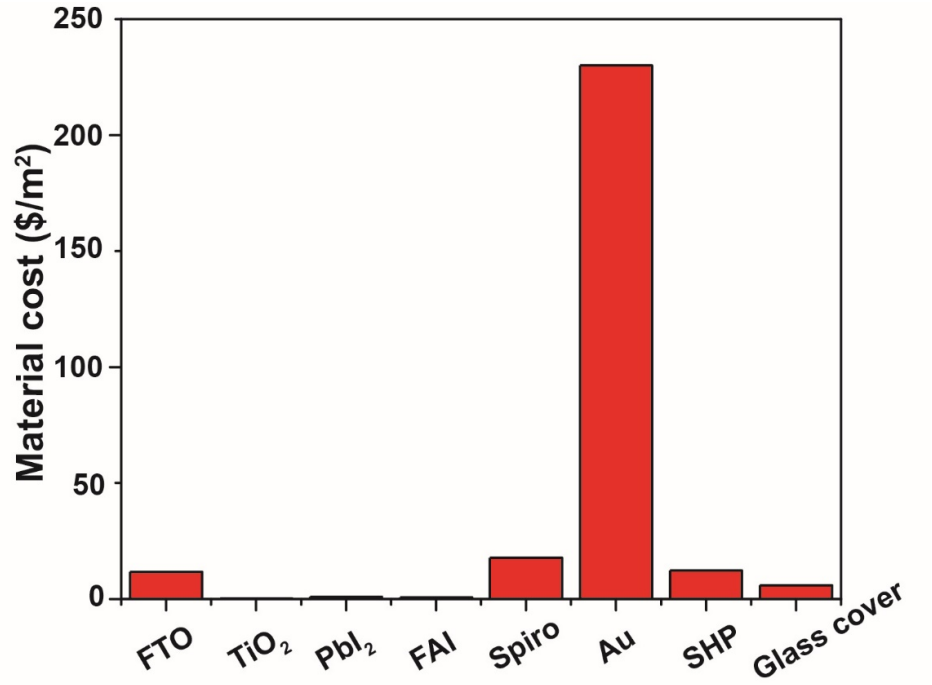

Supplementary Figure 7 | Material cost of the perovskite solar modules. Cost of the self-healing polymer film is similar to the FTO substrate, cheaper than the spiro-MeOTAD and gold electrode layer. Detailed information is shown in Supplementary Table 2.

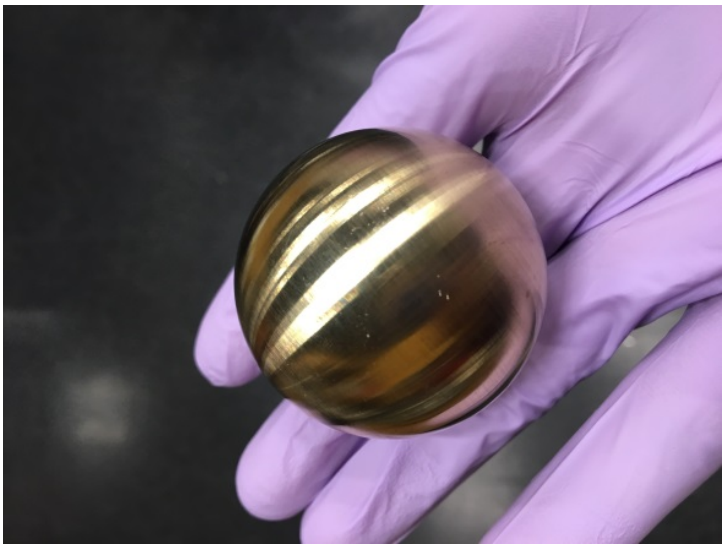

Supplementary Figure 8 | Photograph of the metal ball used for the impact test. The metal ball is chosen according to the standard hail impact test, FM 44787, showing a diameter of 45 mm and a weight of 358 g.

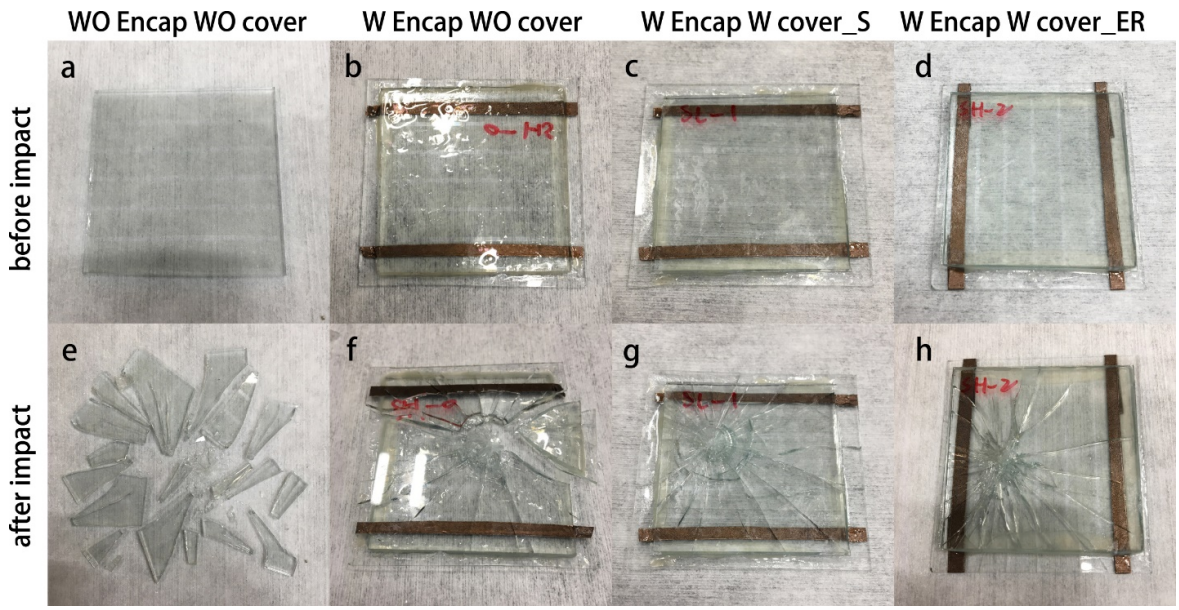

Supplementary Figure 9 | Photographs showing broken patterns for different encapsulation methods. (**a,e**) FTO substrate without encapsulation; FTO substrates encapsulated with (**b,f**) a 1 mm thick glass using a UV-resin on the one side and a ER film on the other side; (**c,g**) a 1 mm-thick glass on one side, a 80 μm-thick surlyn film and 1 mm-thick glass on the other side; (**d,h**) a 1 mm-thick glass on one side, a 80 μm-thick ER film and 1 mm-thick glass on the other side. A distance of 10 cm between the metal ball and the substrate was the optimized distance for achieving star-shaped microcracks.

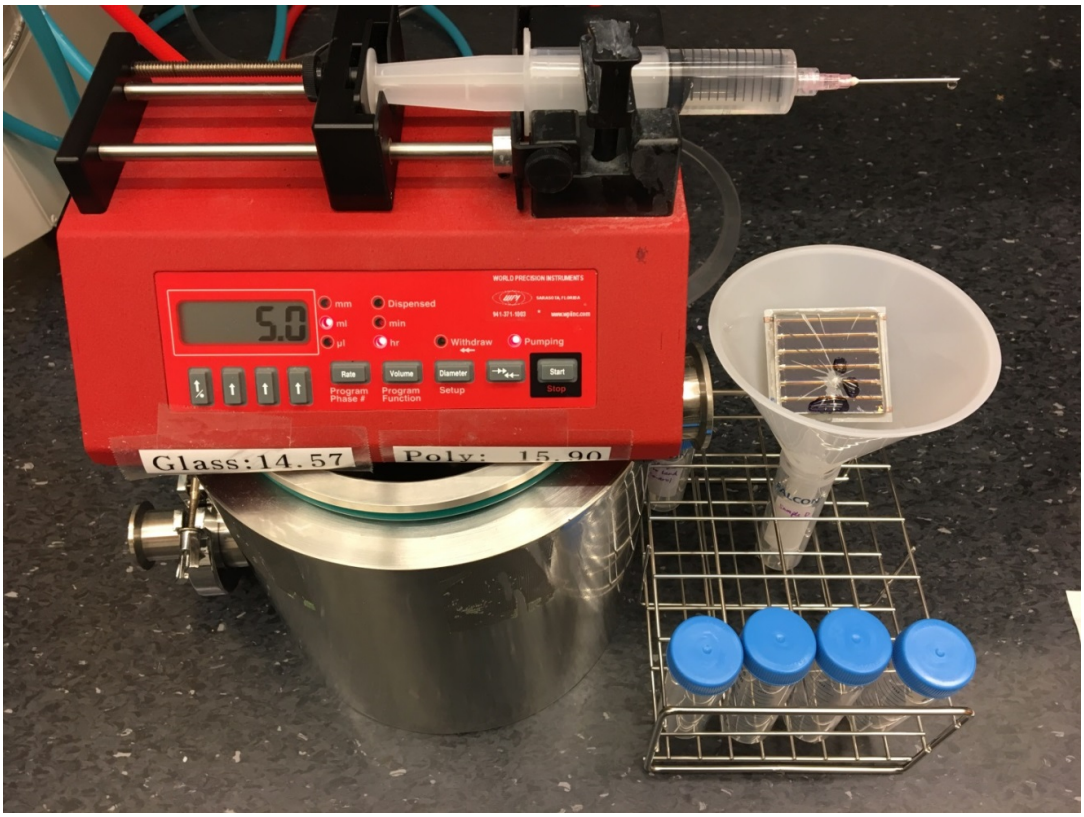

Supplementary Figure 10 | Photograph showing the water dripping test. Acid water (pH = 4.2) was continuously dripped at the damaged part of the perovskite solar module at a speed of 5.0 mL/h for 1.5 h to simulate a heavy acid rain after the perovskite solar module is damaged by natural causes (e.g., hail impact).

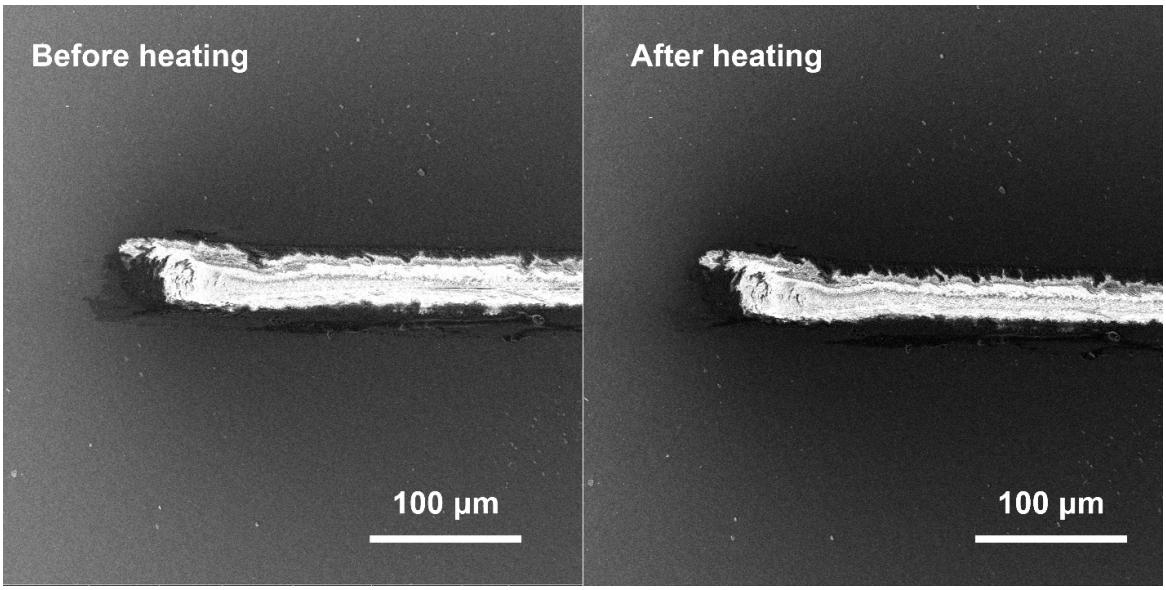

Supplementary Figure 11 | SEM images showing the cutting region of a surlyn film. The surlyn film does not heal after heating treatment.

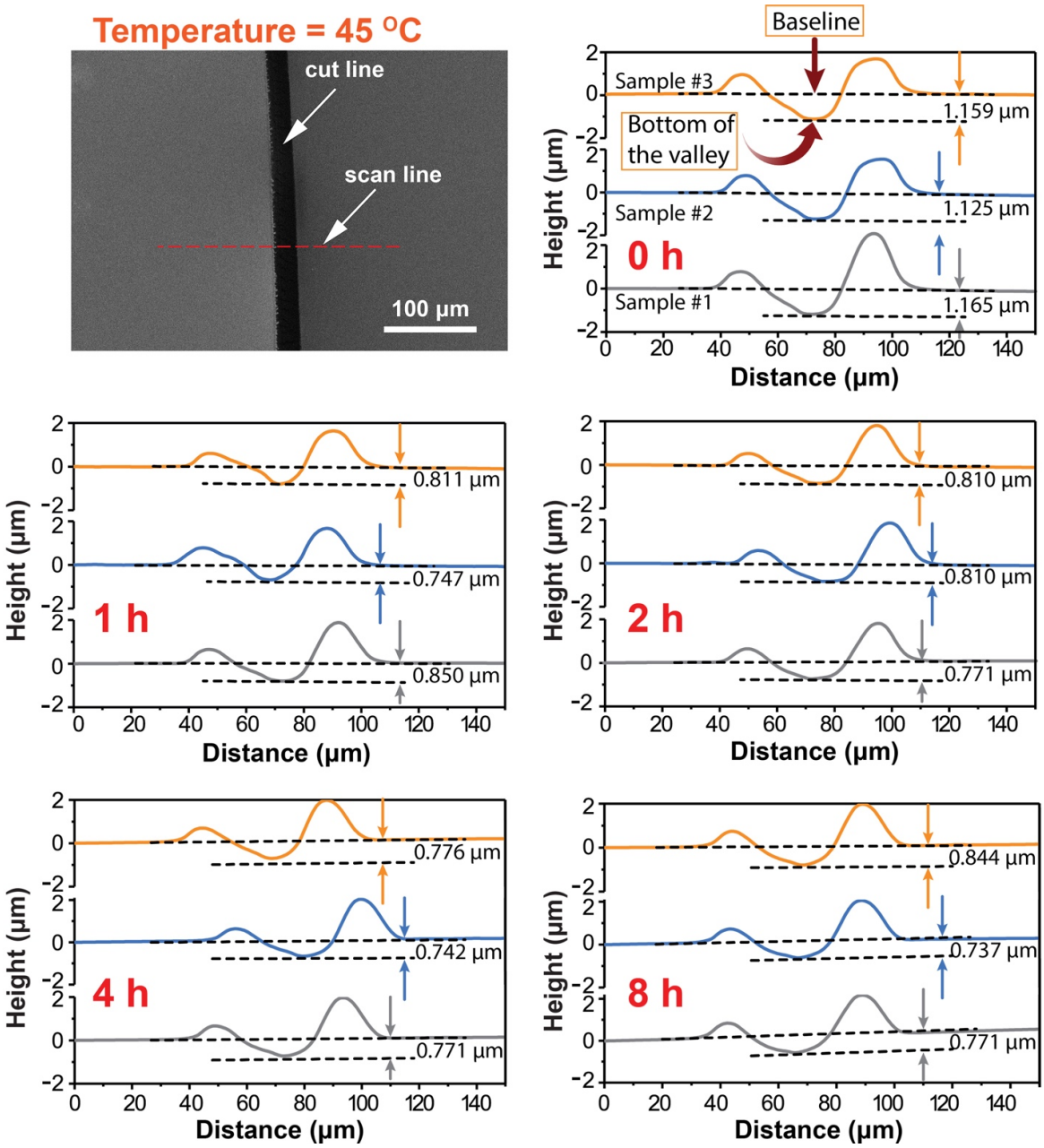

Supplementary Figure 12 | The cut depth on the ER film as a function of heating time at 45 °C. The cutting region of the ER film and the scan line of the profilometer measurement are illustrated in the SEM image on the top left. Here the cut depth is defined as the height difference between the baseline and the bottom of the valley at the cutting region. These values are summarized in Supplementary Table 4 and Figure 4j.

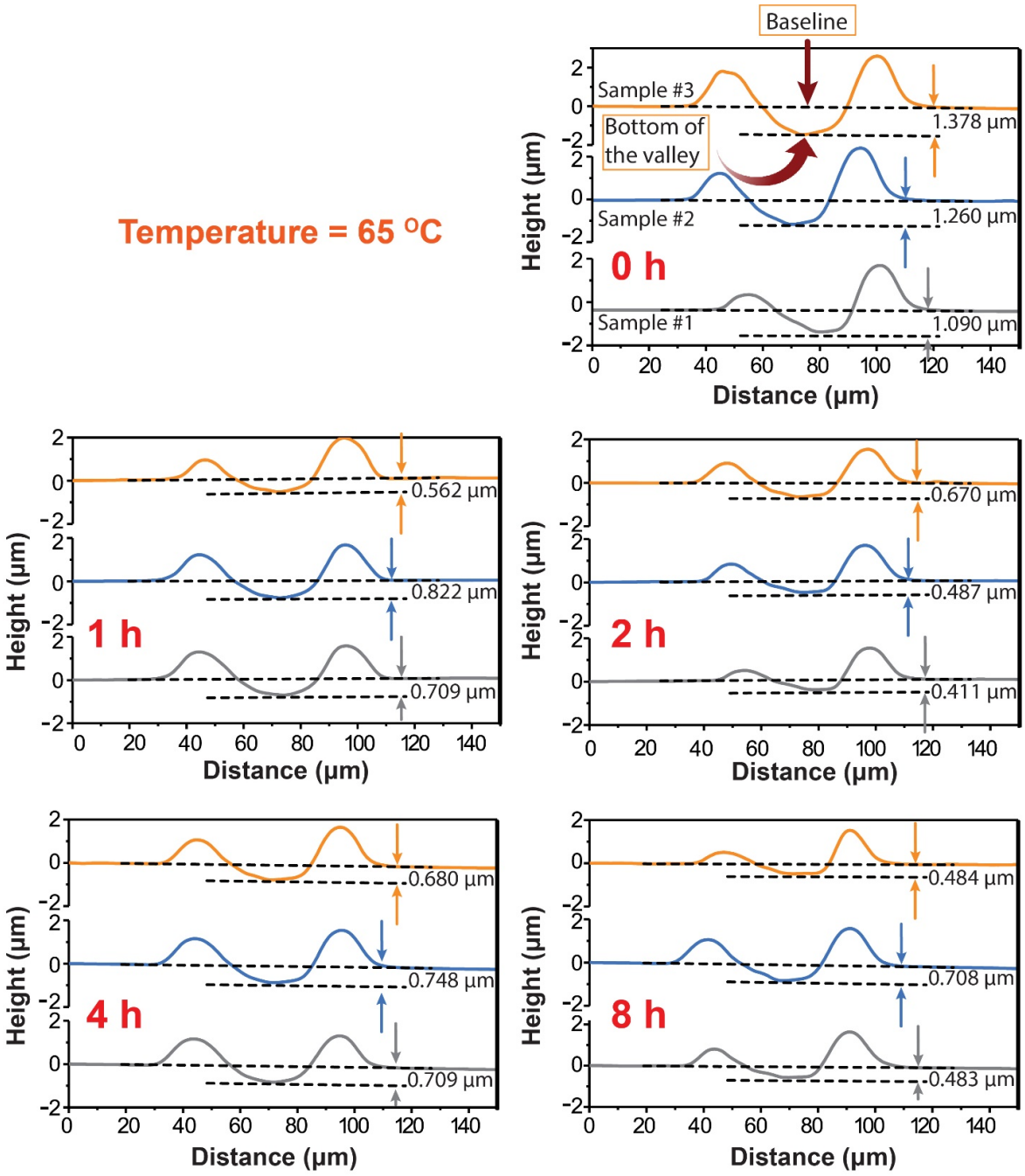

Supplementary Figure 13 | The cut depth on the ER film as a function of heating time at 65 °C. Here the cut depth is defined as the height difference between the baseline and the bottom of the valley at the cutting region. These values are summarized in Supplementary Table 4 and Figure 4j.

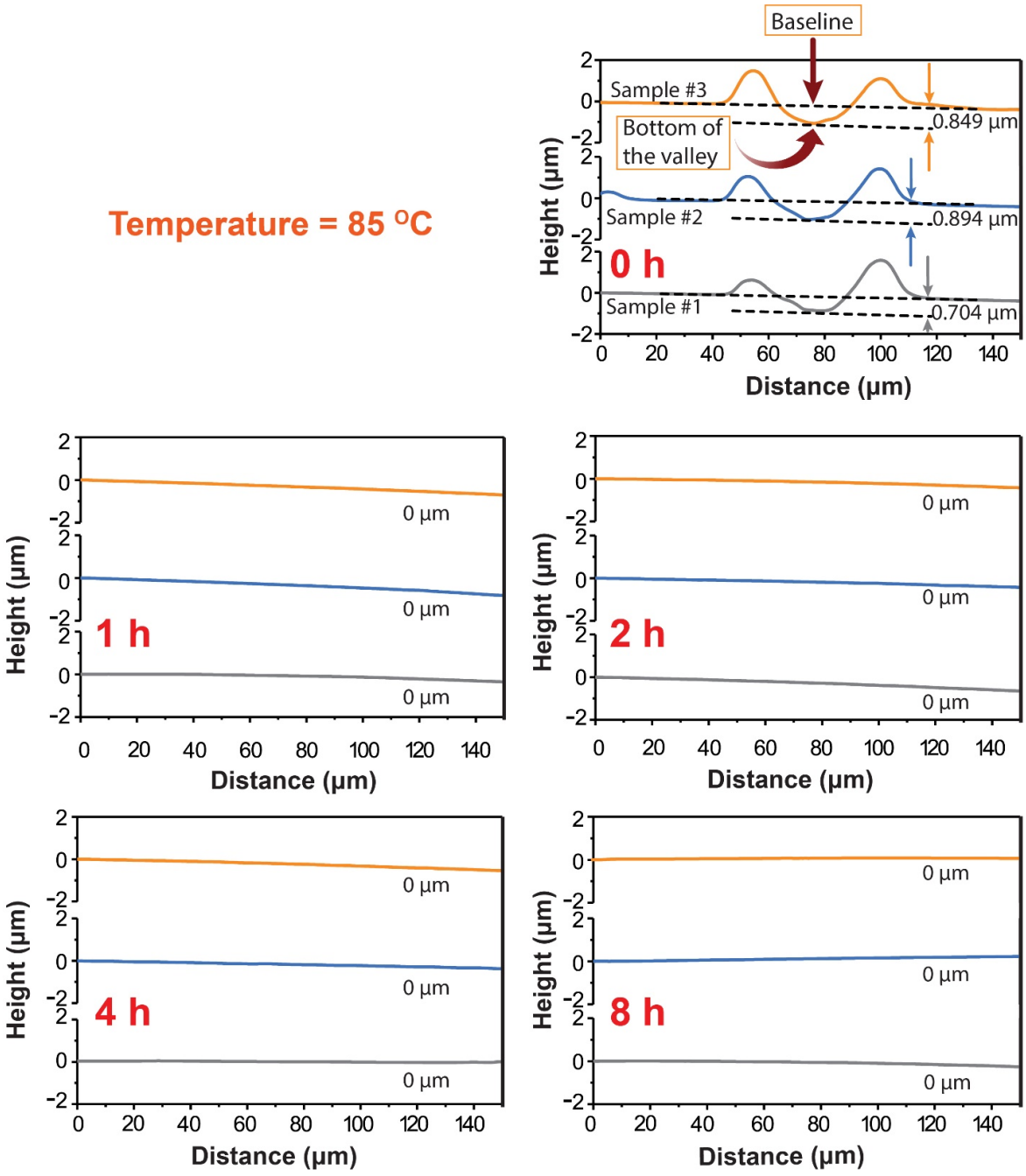

Supplementary Figure 14 | The cut depth on the ER film as a function of heating time at 85 °C. Here the cut depth is defined as the height difference between the baseline and the bottom of the valley at the cutting region. These values are summarized in Supplementary Table 4 and Figure 4j.

Supplementary Tables:

Supplementary Table 1 | Photovoltaic parameters of perovskite solar modules.

Encapsulation method	Sample No.	V_{oc} (V)	J_{sc} (mA/cm^2)	FF (%)	PCE (%)
A	1	5.76	3.66	62.7	13.4
A	2	5.84	3.66	66.9	14.1
A	3	5.8	3.65	61.0	12.9
B	1	5.82	3.63	66.1	14.1
B	2	5.72	3.61	58.4	12.6
B	3	5.77	3.68	60.8	13.2
C	1	5.63	3.03	56.5	9.9
C	2	5.75	3.37	61.6	12.2
C	3	5.69	2.98	55.8	10.7
D	1	5.74	3.73	63.1	13.9
D	2	5.78	3.69	65.2	14.3
D	3	5.72	3.71	60.3	13.2

Supplementary Table 2 | Estimation of the material cost for perovskite solar modules.

Material	unit	Usage (unit/m^2)	Usage ref.	Cost ($/unit)	Material cost ($/$m^2$)	Cost ref.
FTO substrate	m^2	1	[1]	11.7	11.7	[1]
TiO_2	g	3.4	[1]	0.1	0.3	[1]
PbI_2	g	1.4	[1]	0.7	1.0	[1]
FAI	g	0.14	Estimate	4.9	0.7	[2]
Spiro-MeOTAD	g	0.21	Estimate	84.8	17.8	[2]
Au	g	5	[1]	46	230	[1]
Self-healing polymer	g	72.8	Estimate	0.16	12.3	[2]
Glass cover	m^2	1	[1]	5.9	5.9	Estimate

Cost information taken from Ref. [2] is adjusted with the following assumptions: (I) Cost of the materials is reduced to 90% for every doubling of the purchase amount. (II) 10 kg of each material is purchased. With these assumptions, the cost of PbI_2 is 0.7 $/$m^2$, similar to the price shown in Ref. [1]. Usage of FAI is estimated to be similar as MAI shown in Ref. [1]. In order to calculate usage of spiro-MeOTAD and the self-healing polymer, densities are assumed to be 1.06 for spiro-MeOTAD[3] and 0.9 for the self-healing polymer[4]. Cost of the glass cover is assumed to be half of the FTO substrate.

Supplementary Table 3 | Physical parameters of Pb and the estimated A_e values.

Encapsulation method	Experiment No.	D (cm/s)	C_s (kg/m^2)	C_b (kg/m^2)	d (cm)	dm/dt (mg/(h m^2))	dm/dt (kg/s)	A_e (m^2)
A	1	9.45×10^{-6}	1.35×10^{-3}	0	0.2	34	2.36×10^{-11}	3.7×10^{-4}
A	3	9.45×10^{-6}	1.35×10^{-3}	0	0.2	34	2.36×10^{-11}	3.7×10^{-4}
B	1	9.45×10^{-6}	1.35×10^{-3}	0	0.2	31	2.15×10^{-11}	3.4×10^{-4}
B	3	9.45×10^{-6}	1.35×10^{-3}	0	0.2	31	2.15×10^{-11}	3.4×10^{-4}
C	1	9.45×10^{-6}	1.35×10^{-3}	0	0.3	3	2.08×10^{-12}	4.9×10^{-5}
C	3	9.45×10^{-6}	1.35×10^{-3}	0	0.3	3	2.08×10^{-12}	4.9×10^{-5}
D	1	9.45×10^{-6}	1.35×10^{-3}	0	0.3	2	1.38×10^{-12}	3.3×10^{-5}
D	3	9.45×10^{-6}	1.35×10^{-3}	0	0.3	0.08	5.56×10^{-14}	1.3×10^{-6}

Supplementary Table 4 | Cut depth evaluation at the cutting region to illustrate the self-healing properties of the ER film.

Heating temperature (˚C)	**Heating time (h)**	**0**	1	2	4	**8**
	Test	Cut depth (μm)				
45	No. 1	1.165	0.850	0.771	0.771	0.771
	No. 2	1.125	0.747	0.810	0.742	0.737
	No. 3	1.159	0.811	0.810	0.776	0.844
65	No. 1	1.090	0.709	0.411	0.709	0.483
	No. 2	1.260	0.822	0.487	0.748	0.708
	No. 3	1.378	0.562	0.670	0.680	0.484
85	No. 1	0.704	0	0	0	0
	No. 2	0.894	0	0	0	0
	No. 3	0.849	0	0	0	0

Supplementary Table 5 | Simulated Pb leakage amount.

Whether condition	Response time (h)	Pb leaking amount (mg/m^2)			
		Encapsulation Method A	Encapsulation Method B	Encapsulation Method C	Encapsulation Method D
0-4 h rain, 4-72 h no rain	12	1.4×10^2	1.3×10^2	16	7
	72	1.4×10^2	1.3×10^2	16	7
0-72 h rain	12	4.1×10^2	3.9×10^2	48	22
	72	5.4×10^2	5.4×10^2	2.9×10^2	1.3×10^2
0-4 h rain, (total 4 h sun), 48-72 h rain	12	1.4×10^2	1.3×10^2	16	7
	72	5.4×10^2	5.4×10^2	78	9
0-4 h sun, (total 200 h rain)	720	5.4×10^2	5.4×10^2	5.4×10^2	16

Supplementary Note 1.

Photovoltaic performance for perovskite solar modules using different encapsulation methods. To ensure the relevance of this study to the real solar cell applications, the perovskite solar modules used here are all working solar modules with reasonable performance. J-V measurements were performed on a total of 12 encapsulated modules (3 perovskite solar modules for each encapsulation method) to study the effect of encapsulation methods on the module photovoltaic performance. Module PCE is 13.4±0.4% for those without encapsulation (Method A) and 13.3±0.6% for those with only bottom encapsulation (Method B) (Supplementary Table 1), suggesting that the bottom encapsulation has a negligible effect on the module performance. The module PCE significantly decreased to 11±1% for those with the top encapsulation using an 80 μm-thick surlyn adhesive resin and 1 mm-thick glass cover (Method C) (Supplementary Table 1), because of the significantly reduced substrate transparency from the module illumination side especially in the wavelength range between 360 and 600 nm (Supplementary Fig. 3). On the other hand, the module showed an average PCE of 13.8±0.5% for solar modules with encapsulation Method D (Supplementary Table 1), similar to those of Method A and B, due to similar transmittance and reflectance before and after adding the ER film and top glass cover (Supplementary Fig. 3).

Supplementary Note 2.

The ER films show the self-healing properties, i.e., they return from a deformed state (temporary shape) to their original (permanent) shape induced by heating up at temperature higher than the glass transition temperature (Tg).[5,6] As a consequence, the ER films have shown promising applications in manufacturing sensing devices or actuators for medical industries, because of the unique self-healing and easy-processing properties.[7,8] The ER films are formed by mixing diglycidyl ether of bisphenol A type epoxy resin (DGEBA), *n*-octylamine (OA), and m-xylylenediamine (MXDA). The reaction between DGEBA and OA forms linear polymers (Supplementary Fig. 4), which show strong physical crosslinks by tail-to-tail associations among alkyl chains exhibiting the behavior of a physical network.[9,10] By substituting OA with MXDA while maintaining the overall stoichiometric ratio between epoxy and amine, chemical crosslinks are also formed.[6] These chemical crosslinks help improve the mechanical properties of the ER films, which is evidenced by the increased Tg and Tm.[9, 11]

The ER films have the tendency to self-heal when heated up at temperatures higher than Tg (i.e., self-healing), but loses their physical strength when heated up at temperatures higher than their melting temperature (Tm). We determined Tg and Tm of the ER films with three different compositions using differential scanning calorimetry (DSC) (Supplementary Fig. 5a-d). Based on these results, we selected the particular ER (DGEBA: OA: MXDA = 4: 2: 1) with a Tg of 42 °C and Tm of 88 °C as the encapsulant in encapsulation Method D for our Pb leakage study, because such an ER film shows the self-healing properties and maintains desirable physical strength at the temperatures most relevant to solar cell operation. However, we note that the local overheating (known as the hot-spot heating) may occur on the current-limiting cell in a string, causing partial failure of the encapsulation. Therefore, re-adjustment of the polymer composition (e.g., the OA to MXDA ratio) will be needed to increase Tm, especially at the hot regions.

The ER film possesses excellent thermal stability with a thermal degradation temperature of 246.1 °C determined by thermogravimetric analysis (TGA), which is significantly higher than the typical solar cell operating temperature (Supplementary Fig. 6a-d). Activation energy (Ea) corresponding to thermal decomposition of the ER film is 72.6 kJ/mol (Supplementary Fig. 6d).

To demonstrate the feasibility of this encapsulation method, we also evaluated the cost of the ER layer. The price of the 800-μm-thick ER layer is \$12.3/m^2, which amounts to 4.4% of the total cost of the encapsulated perovskite solar modules[1-4], suggesting that it is a promising encapsulant also from the cost point of view. More detailed information for the cost estimation can be found in Supplementary Fig. 7 and Supplementary Table 2.

Supplementary References:

1. Chang. N. *et al*. A manufacturing cost estimation method with uncertainty analysis and its application to perovskite on glass photovoltaic modules. *Prog. Photovolt: Res. Appl.* **25**, 390-405, (2017).

2. *Material cost* (Sigma Aldrich, 2018), *http://sigmaaldrich.com*

3. *Safety data sheet for Spiro-MeOTAD* (Solaronix, 2018), *https://www.solaronix.com/msds/MSDS_Spiro-OMeTAD.pdf*

4. Ma, B., Zhou, X., Wei, K., Bo, Y. & You, Z. Analysis of Preparation and Properties on Shape Memory Hydrogenated Epoxy Resin Used for Asphalt Mixtures. *Appl. Sci.* **7**, 523, (2017).

5. Hager, M. D., Greil, P., Leyens, C., Zwaag, S. V. D. & Schubert, U. S. Self-Healing Materials. *Adv. Mater.* **22**, 5424-5430 (2010).

6. Lv, T. *et al*. Self-Restoration of Superhydrophobicity on Shape Memory Polymer Arrays with Both Crushed Microstructure and Damaged Surface Chemistry. *Small* **13**, 1503402, (2017).

7. Rousseau, I. A. Challenges of Shape Memory Polymers: A Review of the Progress Toward Overcoming SMP's Limitations. *Polym. Eng. Sci*. **48**, 2075-2089 (2008).

8. Lantada, A. D. Systematic Development Strategy for Smart Devices Based on Shape-Memory Polymers. *Polym. Eng. Sci*. **9**, 496 (2017).

9. Xie, T. & Rousseau, I. A. Facile tailoring of thermal transition temperatures of epoxy shape memory polymers. *Polymer* **50**, 1852–1856 (2009).

10. Puig, J. *et al*. Epoxy Networks with Physical Cross-Links Produced by Tail-to-Tail Associations of Alkyl Chains. *Macromolecules* **42**, 9344–9350 (2009).

11. Leonardi, A. B. *et al*. Shape memory epoxies based on networks with chemical and physical crosslinks. *Eur. Polym. J.* **47**, 362-369 (2011).